Journal of Biomolecular Structure & Dynamics, ISSN 0739-1102
Volume 28, Issue Number 6, (2011)

Blocking the DNA Repair System by Traditional Chinese Medicine?

http://www.jbsdonline.com

Mao-Feng Sun [1,2]
Tung-Ti Chang [1,2]
Kai-Wei Chang[1]
Hung-Jin Huang [1]
Hsin-Yi Chen[3]
Fuu-Jen Tsai[3,4]
Jaung-Geng Lin[1]
Calvin Yu-Chian Chen[1,3,5,6]*

[1]Laboratory of Computational and Systems Biology, School of Chinese Medicine, China Medical University, Taichung, 40402, Taiwan
[2]Department of Acupuncture, China Medical University Hospital, Taichung, Taiwan
[3]Department of Bioinformatics, Asia University, Taichung, 41354, Taiwan
[4]Department of Medical Genetics, China Medical University, Taichung, 40402, Taiwan
[5]Department of Systems Biology, Harvard Medical School, Boston, MA 02115, USA
[6]Computational and Systems Biology, Massachusetts Institute of Technology, Cambridge, MA 02139, USA

*Phone: +1-617-353-7123
E-mail: ycc@mail.cmu.edu.tw; ycc929@MIT.EDU (C.Y.-C. Chen)

Abstract

Non-homologous end joining (NHEJ) is a major DNA double strand breaks (DSBs) repair pathway that maintains genome integrity. However, this pathway may reduce radiotherapy efficacy by repairing DSBs on cancer cells. This research reported a computer-aided drug design (CADD) method to identify novel inhibitors from traditional Chinese medicine (TCM) that disrupt NHEJ. We aim to inhibit Ku86, the initiator of NHEJ. By integrating binding energy evaluation and molecular dynamics simulation methods, we reported glycyrrhizic acid, macedonoside C, lithospermic acid, and salvianolic acid B as potential Ku86 inhibitors. All four TCM compounds show low binding energy and stable binding poses to Ku86. The carboxyl groups on a ligand are the major binding region by forming salt bridges at Ku86 binding sites. Additional features were defined by a carbonyl group or a dihydroxyphenyl group that form additional hydrogen bond or pi-cation respectively with the ligand binding site on Ku86. These features strengthen the binding affinity between Ku86 and the potential TCM ligand. We reported all four TCM compounds are potential Ku86 inhibitors and may be used to enhance radiotherapy for cancer treatment.

Key words: Ku protein; Radiotherapy; Traditional Chinese Medicine; Docking; Molecular Dynamics.

Introduction

Radiotherapy is commonly used for the treatment of malignant cancer. The ionizing radiation kills targeted cells through inducing lesion in DNA, such as DNA double strand breaks (DSBs). Non-repaired DNA damages then can lead to cell death. Hence, radiation sensitivity of the target cancerous tumor cells plays an important role in efficacy of radiotherapy (1). Many researches suggest the disruption of non-homologous end joining (NHEJ) pathway, an important DNA repair mechanism, leads to increased radiation sensitivity (2-4). Therefore, target-specific inhibition of NHEJ pathway in cancer cells may lead to enhanced efficacy and specificity of radiotherapy.

Ku protein (Ku86), is one of the key proteins involves in NHEJ pathway (5). Ku86 heterodimer recognizes a DSB site and binds to the broken DNA ends. As shown in Figure 1, the Ku86-DNA complex functions as a moecular scaffold that recruits DNA repair protein assembly, such as DNA-PKcs, XRCC4, and Ligase IV (6). NHEJ ends with the Ligase IV-XRCC4 ligation that rejoins the DSB ends. An active Ku protein contains two subunits, Ku79 and Ku80, which dimerize and form a ring-like structure that has high affinity to DNA broken ends (7, 8). This makes Ku86 not only involves in NHEJ, but also plays a role in telomere maintenance (9, 10). Ku86 deficiency has been linked to high radiosensitivity of cells. Mouse model suggests that deletion of Ku70 or Ku80 lead to hypersensitivity to ionization radiation under

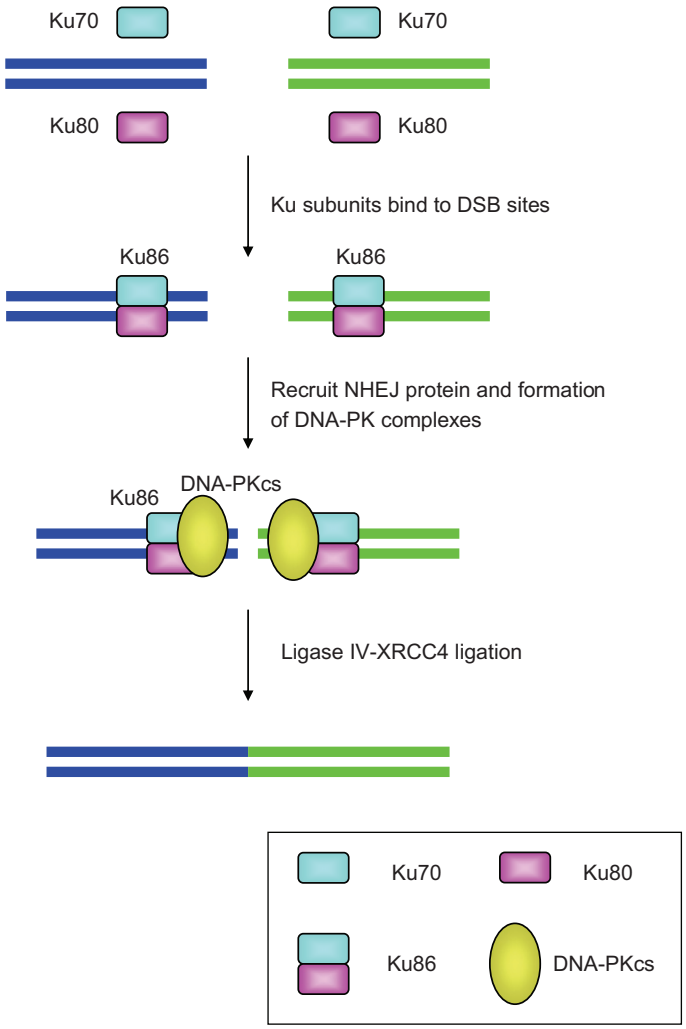

Figure 1: NHEJ pathway diagram. (**A**) Ku70 and Ku80 subunits form Ku86 protein after dimerization. (**B**) Each Ku86 binds to broken DNA ends. (**C**) Ku86 acts as a scaffold for recruiting other NHEJ proteins and form DNA-PKcs. (**D**) Ligase IV-XRCC4 complx is recruited and ligate the broken DNA ends. DNA-repair proteins then diassociate.

a p53 deficient condition (3). In addition, increased expression of Ku70 showed radioresistance in head and neck cancer cell lines (11). Hence, it is possible that inhibition of Ku protein function can abolish NHEJ and thus makes a cell more susceptible to ionizing radiation.

In the past, many potential drug-like compounds targeting proteins such as EGFR, PDE5, influenza hemagglutinin, HER2, HIV enzymes, and more were identified through computer-aid drug design (CADD) (12-27). This study was interested using CADD approaches for discovering novel drug leads that can disrupt NHEJ pathways and therefore enhance radiotherapy efficacy. The research focused on identifying potential Ku86 inhibitors from traditional Chinese medicine (TCM), from which many prospective anti-tumor compounds, such as gallic acid, curcumin, and quercetin, have been identified (28-30). Compounds recorded in TCM database (TCM Database@Taiwan, http://tcm.cmu.edu.tw) (31) were used for *in silico* screening. The selected TCM compounds were further investigated for their interaction with the Ku protein using molecular dynamics (MD) simulation. Both virtual screening and MD simulation were common CADD methods often used for evaluate protein-ligand interactions. Biomedical experiments will be applied to validate each identified Ku heterodimer inhibitors.

Protein Preparation

Ku heterodimer crystal structure was obtained from Protein Data Bank (www.pdb.org PDB ID: 1JEY) (7). Pure protein structural information was extracted from the original pdb file and the missing hydrogen atoms were added. The CHARMm force field was then applied to the Ku protein prior docking or simulation. The DNA binding interface was defined as that ligand docking site. Acetylation and mutagenesis studies on Lys282, Lys338, Lys539 and Lys542 at Ku70 have been demonstrated to suppress the DNA end-binding activity (32). In this study, Lys282 and Lys338 were the only two residues presents in the 1JEY crystal file, and hence were investigated further.

Docking

A total of 20,000 isolated products from TCM were obtained from the TCM Database@Taiwan (http://tcm.cmu.edu.tw/) (31), where each compound was ionized according to the physiological setting, using Discovery Studio 2.5. These compounds were also filtered using ADMET module in Discovery 2.5 to remove any potentially toxic compounds. LigandFit module in Discovery Studio 2,5 was applied to evaluate the binding energy between each TCM compound and DNA binding region of the Ku protein (33). Monte Carlo simulation was used to generate ligand conformations using a shape-based matching method. The docking site was held rigid for trying out ligand binding poses. Ligand conformations were energetically minimized using Smart Minimizer. Ligands were ranked according to the Binding Energy, which represents the binding affinity. In addition, LigScore (LigScore1 and LigScore2) and piecewise linear potential (-PLP and -PLP2) were applied to evaluate binding affinities. Binding Energy evaluates the free energy in a protein-ligand conformation. LigScore computes softened van der Waal descriptor and polar surface area descriptors (34). LigScore2 differs from LigScore by the introduction of desolvation penalty. The piecewise linear potential calculate hydrogen bond interactions between hydrogen bond donor, hydrogen bond acceptor, and non-polar atom types (35). The PLP2 function further includes a scaling factor based on the angles between receptor atoms and ligand atoms. Top ranking TCM candidates were visually inspected to identify ligands that interact with key residues, Lys282 and Lys338 of Ku70.

Molecular Dynamics Simulation

Molecular dynamics (MD) simulation was applied to the selected protein-ligand complexes using the simulation module in Discovery Studio 2.5. Each complex was solvated in a simulated water box with 0.9% NaCl concentration, which corresponds to physiological solution. Periodic boundary condition was applied. The initial minimization process consisted 2000 steps of Steepest Descent and 2000 steps of Conjugate Gradient. The system was heated from 50 K to 310 K without constraint within 20 ps with a time step of 1fs. The equilibration step was run for 100 ps at 310 K. The production was run under constant temperature condition (NVT) for 10 ns at 310 K. SHAKE algorithm was then applied to constraint bindings to hydrogen atoms. Root mean square deviations (RMSDs) were calculated for both protein-ligand complexes and ligands.

Results

Identification of TCM Candidates from Screening TCM Database

Molecular docking was performed to screen for potential Ku protein inhibitors from the TCM database. Binding energy was employed to evaluate the protein-ligand

Table I

TCM molecules docking result. The top 10 candidates are listed and calculated binding energy.

Name	Binding energy (kcal/mol)
Glycyrrhizic acid	-732.092
Macedonoside C	-691.639
Lithospermic acid	-527.754
Salvianolic acid B	-525.367
Mumefural	-514.916
Chicoric_acid	-504.861
2-O-Feruloyl tartaric acid	-492.562
Crocetin	-449.829
Glutinic acid	-424.322
Chebulinic acid	-419.415

binding affinities. The screening results listed in Table 1 suggests that glycyrrhizic acid (top 1), macedonoside C (top 2), lithospermic acid (top 3), and salvianolic acid B (top 4) can form stable binding conformations at low energy stage, between -525.367 kcal/mol and -732.092 kcal/mol, with the DNA binding site on the Ku86 heterodimer. The ligands shared structural similarities between top1 and top2, and betweem top3 and top4 (Figure 2). For glycyrrhizic acid and macedonoside C, negative charges of the carboxyl groups favored the bindings to the Ku86 DNA-binding domain, where most key residues contained positive charges (Figures 2 and 3). The binding conformations suggested that a hydrogen bond (H-bond) was the major intermolecular force in the protein-ligand binding (Figure 4). Glycyrrhizic acid and macedonoside C can be extracted from licorice (*Glycyrrhiza glabra*), which is a common TCM herb used in many formulations (36, 37). In the case of lithospermic acid, and salvianolic acid B, less carboxyl groups (Figure 2) implied fewer instances of H-bonds observed. Nevertheless, the negative electrostatic potential on the top 3 and the top 4 compounds still favored the alkaline residues in Ku86 ligand binding site (Figures 2 and 3). Intriguingly, the binding affinity between Ku86 and each of these ligands were strengthened by the pi-cation interactions (Figure 4). Lithospermic acid, and salvianolic acid B are extracts of Salvia miltiorrhiza, which is commonly used for circulation disorders in TCM.

Ligands Bind to Ku84 DNA Binding Site Through Formation of Salt Bridge

The protein-ligand binding conformation in Figure 4 and Table 2 suggested a binding hot spot on Ku86 heterodimer at Ku70: Arg403 and Ku70: Lys338. Furthermore, the binding conformation of glycyrrhizic acid, lithospermic acid, and salvianolic acid B on Ku86 shares similar binding position. The binding conformations revealed that the carboxyl groups on these ligands formed H-bond with residues Ku70: Lys338, Ku70: Glu335, and Ku80: Arg446. In addition, the H-bond and the electrostatic interaction between oxygen and nitrogen, which in combination was defined as a salt bridge, made positive contribution to the binding affinity at Ku70: Lys338, Ku70: Glu335 (Figure 4). However, macedonoside C bound to

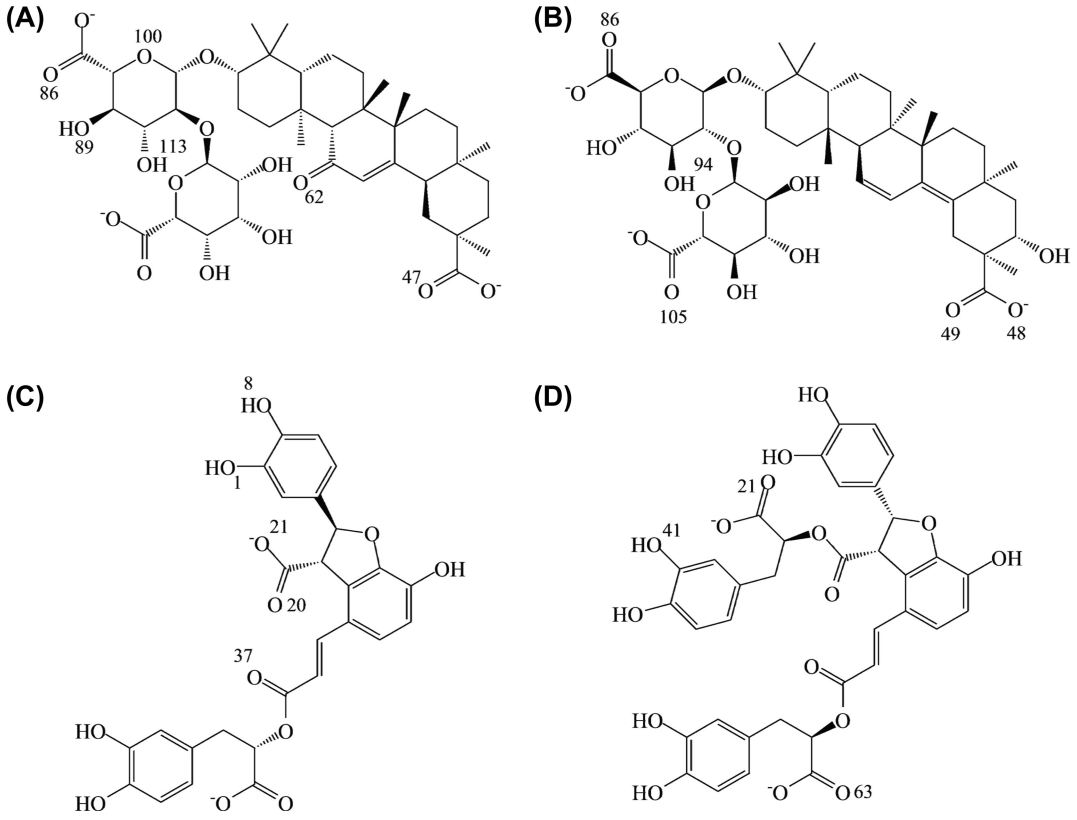

Figure 2: Chemical structures of (**A**) Glycyrrhizic acid, (**B**) Macedonoside C, (**C**) Lithospermic acid, (**D**) Salvianolic acid B.

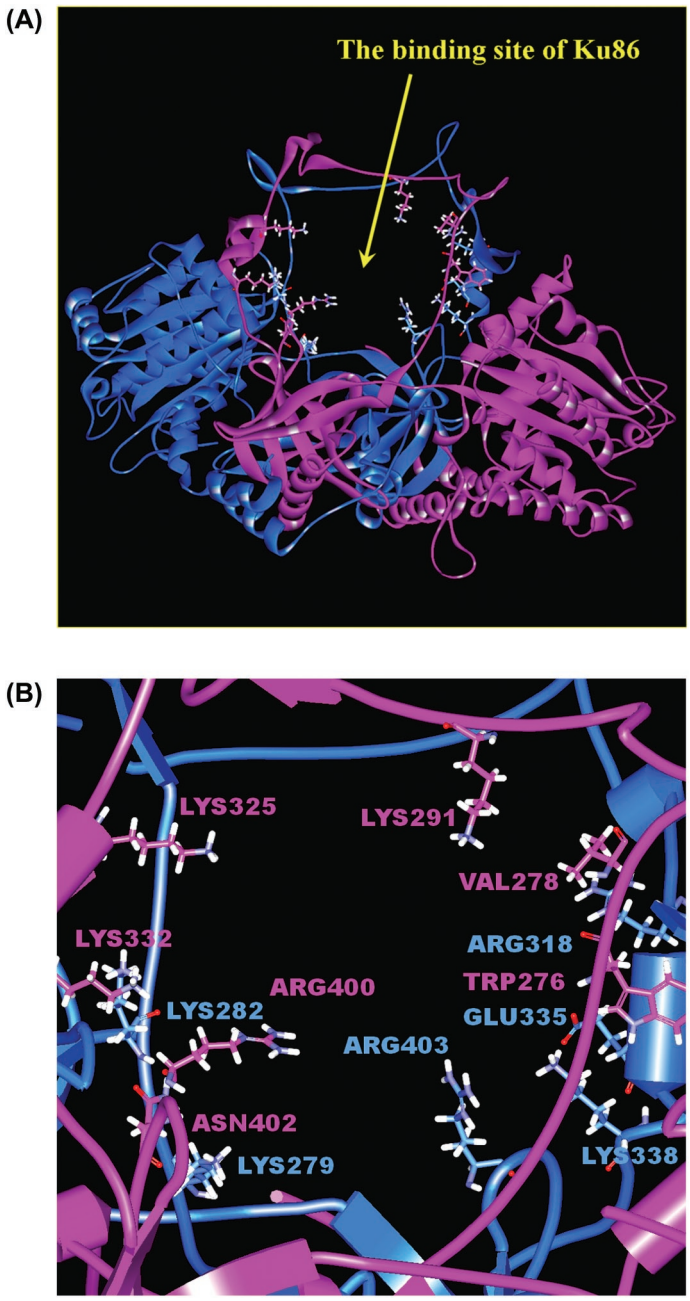

Figure 3: Ku heterodimer DNA-binding site, and presumed inhibitor binding site. (**A**) The ring structure Ku heterodimer DNA-binding site. (**B**) Close look of binding site, where key binding site residues were shown. The Ku70 and the Ku80 subunits and residues are colored in blue and purple, respectively.

a distinct set of residues, which concentrated at Ku80 subunit, at Lys265, Arg271, and Lys332. Despite the distinct binding poses, the salt bridges formed between carboxyl group and the alkaline residues are the major interaction for the Ku-ligand binding affinity.

Stable RMSD Trajectories Suggest Stable Ku-ligand Bindings During MD Simulation

The molecular docking provided a static protein-ligand model for predicting a preferred binding orientation. To further evaluate the binding poses in motion, we applied molecular dynamics (MD) simulation for 10ns on each of the selected Ku-ligand pair. The RMSD trajectories for Ku-ligand complex, C-alpha, and ligand of each binding pair were investigated and showed stable poses which the average atom movements were under 1Å range (Figure 5). This implied relatively stable bindings

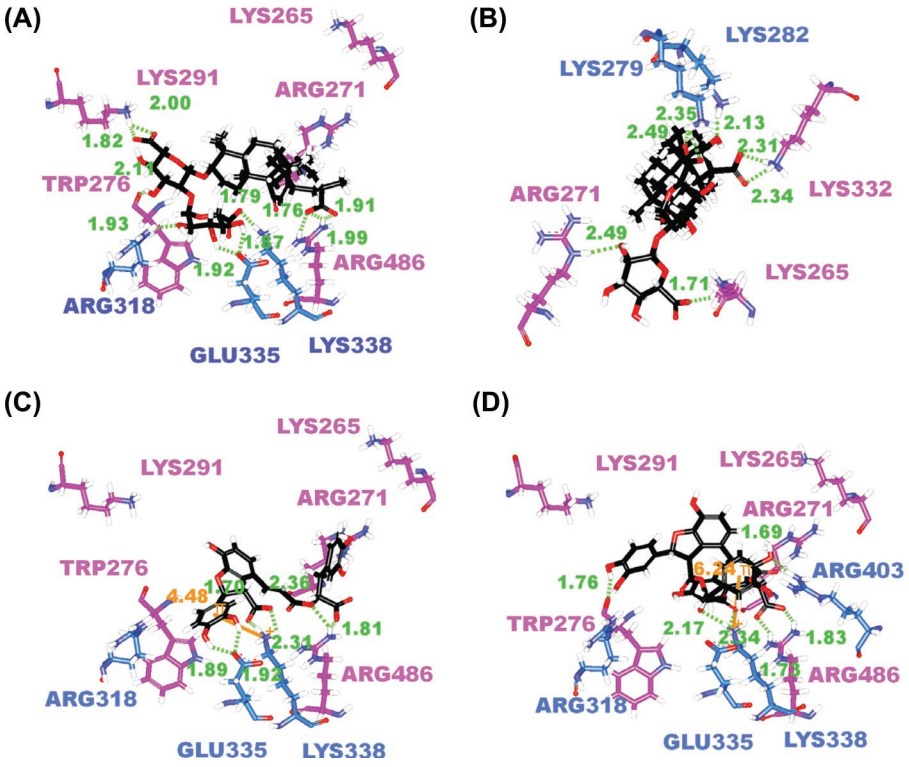

Figure 4: The docking poses of (**A**) Glycyrrhizic acid, (**B**) Macedonoside C, (**C**) Lithospermic acid, (**D**) Salvianolic acid B in Ku 86 binding site. Residues on Ku70 and Ku80 are colored in blue and purple respectively. The pi-cation interaction is indicated in orange line.

between Ku86 and the selected ligands from molecular docking. Intriguingly, the ligand RMSD showed that lithospermic acid experienced a leap of change for over 1 Å at 5-6ns of the simulation period before stabilizing (Figure 5). However, the complex and protein RMSD displayed no significant change over the same period. This implied the change in the ligand pose of lithospermic acid had limited impact on protein-ligand interaction. By tracking the changes in total energy (Figure 6), glycyrrhizic acid and macedonoside C reached minimum energy state at around 5ns

Table II

Hydrogen bond frequency of top 4 TCM candidates during 10 ns simulation. Residues from Ku70 subunit and Ku80 subunits were included.

Compound	Ligand Atom	Subunit	Amino Acid	H-Bond Occupancy
Glycyrrhizic acid	O100	Ku70	ARG318 : HE	75.60%
	H113	Ku70	GLU335 : OE2	52.00%
	O47	Ku70	LYS338 : HZ3	43.20%
	O62	Ku70	ARG403 : HH12	86.80%
	O89	Ku80	VAL278 : HN	77.60%
	O86	Ku80	LYS291 : HZ1	65.60%
Macedonoside C	O105	Ku70	LYS279 : HZ1	67.20%
	O48	Ku80	LYS325 : HZ3	63.20%
	O49	Ku80	LYS325 : HZ3	61.60%
	O86	Ku80	LYS332 : HZ1	77.20%
	H94	Ku80	ARG400 : O	100.00%
Lithospermic acid	H8	Ku70	GLU335:OE2	98.00%
	O1	Ku70	ARG403:HH22	71.20%
	O21	Ku70	LYS338:HZ1	42.40%
	O37	Ku80	ARG271:HH11	88.00%
	O20	Ku80	ARG486:HH22	88.80%
Salvianolic acid B	O63	Ku70	ARG403:HH21	77.20%
	O21	Ku70	LYS338:HZ1	62.40%
	O21	Ku70	LYS338:HZ3	86.00%
	O41	Ku80	VAL278:HN	16.00%

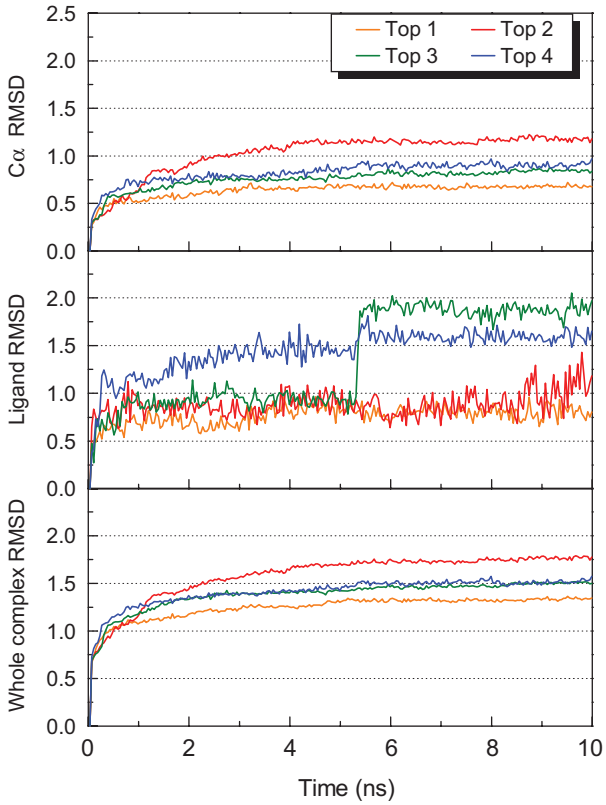

Figure 5: The RMSD value (Å) of Ku-ligand complexes for top 4 TCM candidates. Top 1 to Top 4 compounds represent glycyrrhizic acid, macedonoside C, lithospermic acid, and salvianolic acid B respectively.

and 6ns simulation time respectively. All four selected TCM compounds reached minimum energy after 8ns, and hence implied stable Ku-ligand complexes.

MD Simulation show Stabilization of Ku-ligand Interaction Through Persistent Hydrogen Bonds

To further investigate the binding poses during MD simulation, we compared the structure snapshots at a set of selected time points. For glycyrrhizic acid, the

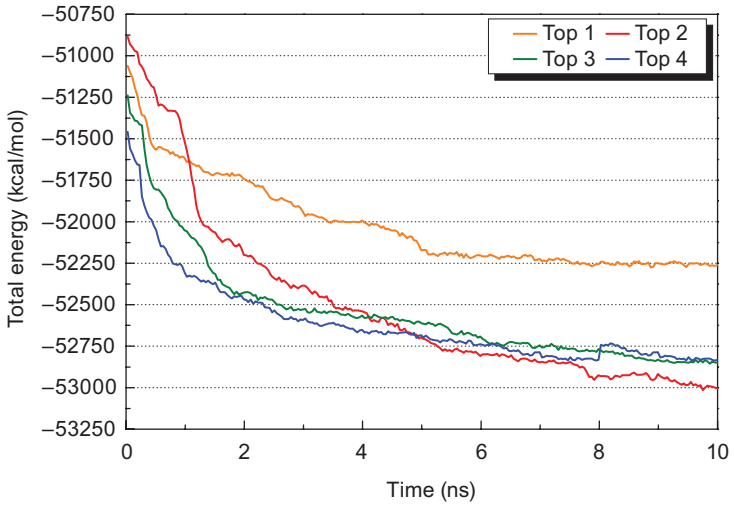

Figure 6: Total energy of each Ku-ligand complex for selected TCM candidates. Top 1 to Top 4 compounds represent glycyrrhizic acid, macedonoside C, lithospermic acid, and salvianolic acid B respectively.

carbonyl group O_{62} moved close to Ku70: Arg403 at range of 2.0-2.5 Å during MD simulation (Figures 4A, and 7). Furthermore, the calculated H-bond occupancy was 86.80% (Table II). These observations implied formation of a new H-bond that was not observed from molecular docking. Glycyrrhizic acid also periodically formed H-bonds with Glu335 and Lys338 at Ku70 subunit (Figure 7, supplementary video 1) during the 10 ns MD simulation, suggesting possible presence of polar interactions that maintain the binding conformation.

Macedonoside C has a distinct binding conformation to Ku86, and the ligand favored interaction with Ku80 subunit. During MD simulation, all three carboxyl groups on macedonoside C formed salt bridges with the lysine residues, Ku70: LYS279, Ku80: LYS325, and Ku80: LYS332 at Ku86 DNA-binding site (Figure 4, Table II). It is possible that the missing carbonyl O_{62} on macedonoside C decreased the ligand binding affinity to Ku70 subunit, and resulted in a distinct binding conformation compare to Ku-glycyrrhizic acid complex. Nevertheless, most H-bonds in Ku-macedonoside C remained stable with occupancies maintained at range 61.60%-77.20% (Table II) A notable stable H-bond was observed at Ku80: Arg400, which maintained a 100% H-bond occupancy to the ligand, in spite of conformation change on the same residue (supplementary video 2). The hydrogen bonding interaction on each alkaline residue stabilized near the end of MD simulation (Figure 8). These analysis presented stable molecular interactions between ligand and the key residues.

The MD simulation on lithospermic acid and salvianolic acid binding conformations revealed that Ku70: Lys338 and Ku70: Arg403 were potential binding residues on the Ku86 DNA-binding site. Both alkaline residues were found to form salt bridges with the carboxyl groups on each ligand. The high H-bond occupancies observed (Table II) and the decreasing hydrogen bonding distances over time

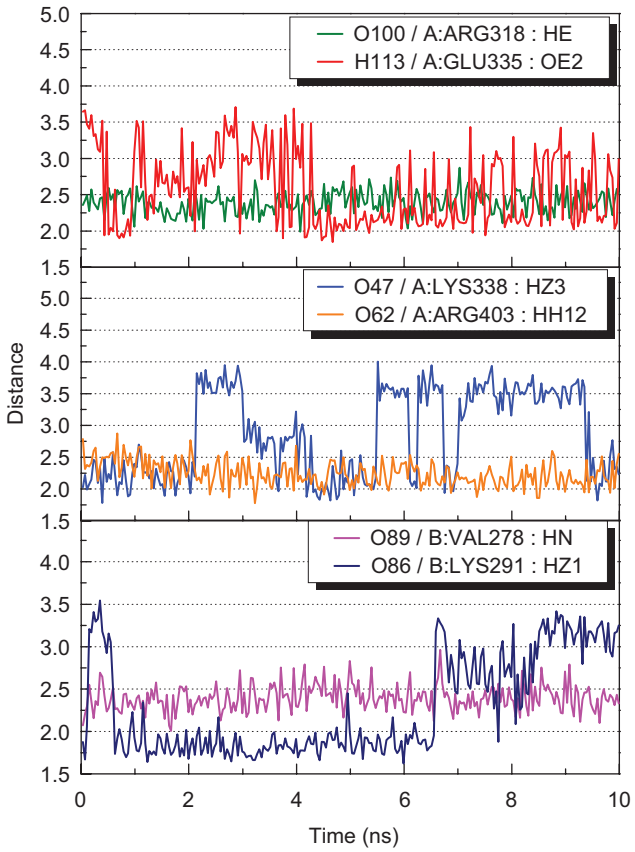

Figure 7: Hydrogen bond distances of Glycyrrhizic acid during 10 ns simulation.

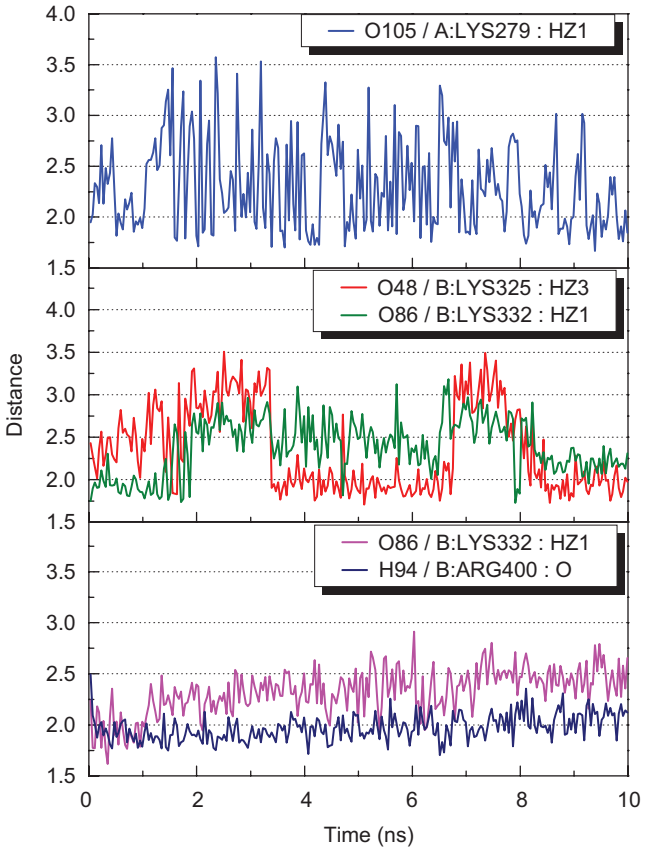

Figure 8: Hydrogen bond distances of Macedonoside C during 10 ns simulation.

during MD simulations (Figures 9 and 10) implied stable molecular interactions on these potential residues. We further investigated the RMSD leaps observed around 5-6ns with regard to the lithospermic acid MD simulation (Figure 5). The conformation analysis (Figure 11, supplementary video 3) revealed that the Ku80: Arg486

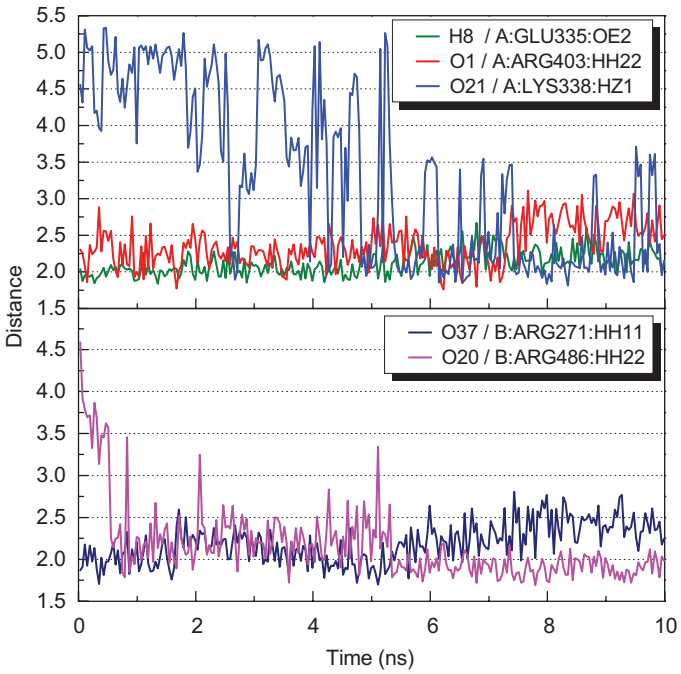

Figure 9: Hydrogen bond distances of Lithospermic acid during 10 ns simulation.

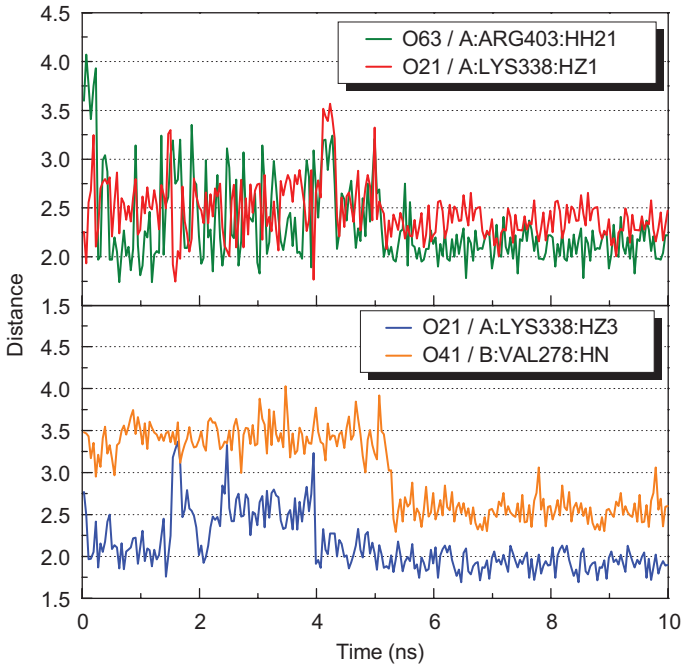

Figure 10: Hydrogen bond distances of Salvianolic acid B during 10 ns simulation.

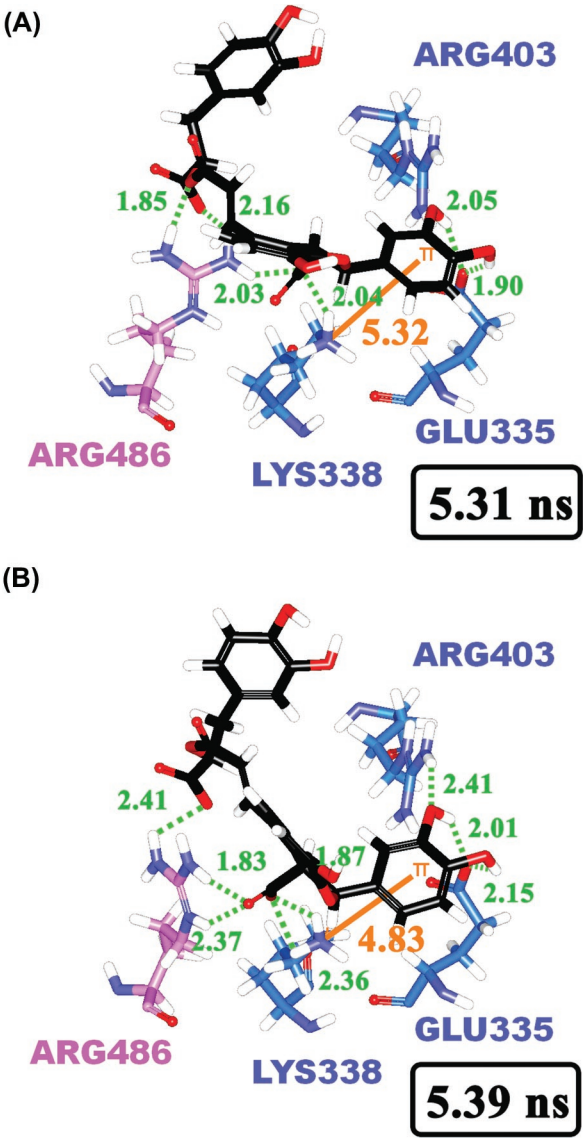

Figure 11: Snapshots of lithospermic acid in Ku binding site at (**A**) 5.31 ns and (**B**) 5.39 ns. Residues of Ku70 and Ku80 are colored in blue and purple, respectively.

pose was altered and pulled the ligand carboxyl group closer and formed more H-bonds that resulted conformation change on lithospermic acid within the binding site. In addition, the conformation change moved the ligand dihydroxyphenyl group closer to the Ku70: Lys338, from 5.32 Å to 4.83 Å, and result high pi-cation binding affinity. Hence, the observed RMSD leap may imply a conformation change that further stabilize the protein-ligand binding.

Conclusion

The alkaline residues on Ku86 DNA binding site plays important role in ligand binding. In particular, the Lys338 and Arg403 on Ku70 subunit were the binding hot spots for interacting with glycyrrhizic acid, lithospermic acid, and salvianolic acid B. On the other hand, macedonoside C lacked a carbonyl group, which was required to form H-bond with Ku70: Arg403, and results stronger interaction with Ku80 subunit of the Ku heterodimer. Nevertheless, the three carboxyl groups on macedonoside C form stable H-bonds with the alkaline residues on Ku80 subunit, which results stable binding conformation. Based on the CADD design, an efficient Ku86 inhibitor is expected to form strong binding affinity with both Lys338 and Arg403 on Ku70 subunit. Figure 12 demonstrated that the carboxyl groups played a major role in protein-ligand interaction. Moreover, the carbonyl group (Figure 12A) and the dihydroxyphenyl group (Figure 12B) that formed additional H-bond and pi-cation interaction respectively were the key features for stable Ku86-ligand binding. The selected TCM compounds, glycyrrhizic acid, macedonoside C, lithospermic acid, and salvianolic acid B, demonstrated low binding energy and formation of stable Ku86-ligand complexes. We conclude that all four compounds are potential enhancers for radiotherapy.

Supplementary Material

Supplementary videos of the MD simulations are displayed at the website of the article at jbsdonline.com.

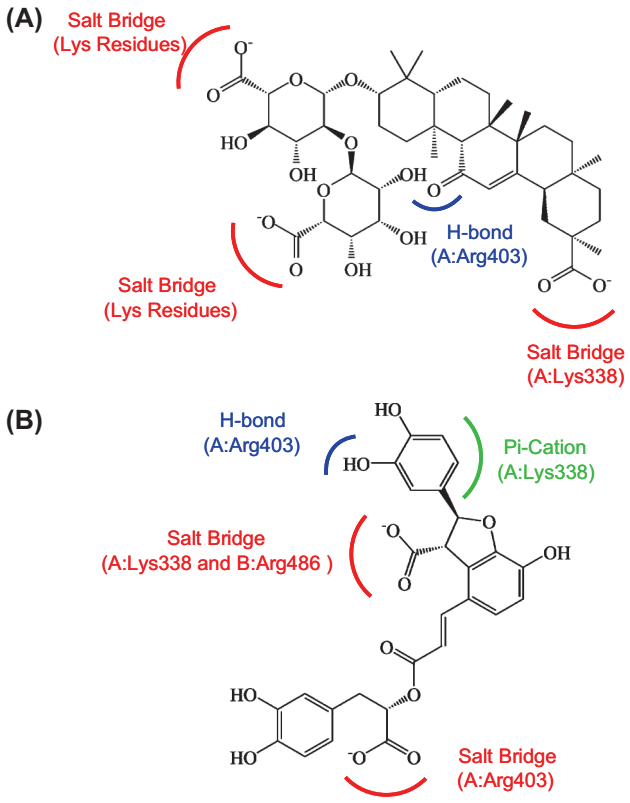

Figure 12: Key features for Ku86 drug design. The common features of (**A**) top1 and top2 compounds; and (**B**) top 3 and top 4 compounds were included. Salt bridges (red), H-bonds (blue), and Pi-Cation (green) interactions were demonstrated.

Acknowledgements

The research was supported by grants from the National Science Council of Taiwan (NSC 99-2221-E-039-013-), China Medical University (CMU98-TCM, CMU99-S-02) and Asia University (CMU98-ASIA-09). This study is also supported in part by Taiwan Department of Health Clinical Trial and Research Center of Excellence (DOH100-TD-B-111-004) and Taiwan Department of Health Cancer Research Center of Excellence (DOH100-TD-C-111-005). We are grateful to the National Center of High-performance Computing for computer time and facilities.

References

1. J. Thoms and R. G. Bristow. *Semin Radiat Oncol 20*, 217-222 (2010).
2. Z. E. Karanjawala, N. Adachi, R. A. Irvine, E. K. Oh, D. Shibata, K. Schwarz, C. L. Hsieh, and M. R. Lieber. *DNA Repair (Amst) 1*, 1017-1026 (2002).
3. D. S. Lim, H. Vogel, D. M. Willerford, A. T. Sands, K. A. Platt, and P. Hasty. *Mol Cell Biol 20*, 3772-3780 (2000).
4. T. Leong, M. Chao, S. Bassal, and M. McKay. *Br J Cancer 88*, 1251-1255 (2003).
5. M. H. Yun and K. Hiom. *Nature 459*, 460-463 (2009).
6. B. L. Mahaney, K. Meek, and S. P. Lees-Miller. *Biochem J 417*, 639-650 (2009).
7. J. R. Walker, R. A. Corpina, and J. Goldberg. *Nature 412*, 607-614 (2001).
8. A. Rivera-Calzada, L. Spagnolo, L. H. Pearl, and O. Llorca. *EMBO Rep 8*, 56-62 (2007).
9. H. L. Hsu, D. Gilley, E. H. Blackburn, and D. J. Chen. *Proc Natl Acad Sci USA 96*, 12454-12458 (1999).
10. G. B. Celli, E. L. Denchi, and T. de Lange. *Nat Cell Biol 8*, 885-U162 (2006).
11. H. W. Chang, S. Y. Kim, S. L. Yi, S. H. Son, Y. Song do, S. Y. Moon, J. H. Kim, E. K. Choi, S. D. Ahn, S. S. Shin, K. K. Lee, and S. W. Lee. *Oral Oncol 42*, 979-986 (2006).
12. A. M. Andrianov. *J Biomol Struct Dyn 26*, 445-454 (2009).
13. A. M. Andrianov and I. V. Anishchenko. *J Biomol Struct Dyn 27*, 179-193 (2009).
14. M. T. Cambria, D. Di Marino, M. Falconi, S. Garavaglia, and A. Cambria. *J Biomol Struct Dyn 27*, 501-509 (2010).

15. C. Y. Chen. *J Biomol Struct Dyn 27*, 627-640 (2010).
16. C. Y. Chen, Y. H. Chang, D. T. Bau, H. J. Huang, F. J. Tsai, C. H. Tsai, and C. Y. C. Chen. *J Biomol Struct Dyn 27*, 171-178 (2009).
17. E. F. F. da Cunha, E. F. Barbosa, A. A. Oliveira, and T. C. Ramalho. *J Biomol Struct Dyn 27*, 619-625 (2010).
18. L. I. D. Hage-Melim, C. H. T. D. da Silva, E. P. Semighini, C. A. Taft, and S. V. Sampaio. *J Biomol Struct Dyn 27*, 27-35 (2009).
19. H. J. Huang, K. J. Lee, H. W. Yu, C. Y. Chen, C. H. Hsu, H. Y. Chen, F. J. Tsai, and C. Y. C. Chen. *J Biomol Struct Dyn 28*, 23-37 (2010).
20. H. J. Huang, K. J. Lee, H. W. Yu, H. Y. Chen, F. J. Tsai, and C. Y. Chen. *J Biomol Struct Dyn 28*, 187-200 (2010).
21. A. K. Kahlon, S. Roy, and A. Sharma. *J Biomol Struct Dyn 28*, 201-210 (2010).
22. C. Koshy, M. Parthiban, and R. Sowdhamini. *J Biomol Struct Dyn 28*, 71-83 (2010).
23. S. Mohan, J. J. P. Perry, N. Poulose, B. G. Nair, and G. Anilkumar. *J Biomol Struct Dyn 26*, 455-464 (2009).
24. J. Sille and M. Remko. *J Biomol Struct Dyn 26*, 431-444 (2009).
25. Y. Tao, Z. H. Rao, and S. Q. Liu. *J Biomol Struct Dyn 28*, 143-158 (2010).
26. L. H. Zhong and J. M. Xie. *J Biomol Struct Dyn 26*, 525-533 (2009).
27. T. T. Chang, H. J. Huang, K. J. Lee, H. W. Yu, H. Y. Chen, F. J. Tsai, M. F. Sun, and C. Y. Chen. *J Biomol Struct Dyn 28*, 309-321 (2010).
28. C. C. Su, J. S. Yang, C. C. Lu, J. H. Chiang, C. L. Wu, J. J. Lin, K. C. Lai, T. C. Hsia, H. F. Lu, M. J. Fan, and J. G. Chung. *Phytother Res 24*, 189-192 (2010).
29. C. Lo, T. Y. Lai, J. H. Yang, J. S. Yang, Y. S. Ma, S. W. Weng, Y. Y. Chen, J. G. Lin, and J. G. Chung. *Int J Oncol 37*, 377-385 (2010).
30. S. H. Wu, L. W. Hang, J. S. Yang, H. Y. Chen, H. Y. Lin, J. H. Chiang, C. C. Lu, J. L. Yang, T. Y. Lai, Y. C. Ko, and J. G. Chung. *Anticancer Res 30*, 2125-2133 (2010).
31. C. Y. C. Chen. *PLoS ONE 6*, e15939 (2011).
32. C. S. Chen, Y. C. Wang, H. C. Yang, P. H. Huang, S. K. Kulp, C. C. Yang, Y. S. Lu, S. Matsuyama, C. Y. Chen, and C. S. Chen. *Cancer Res 67*, 5318-5327 (2007).
33. C. M. Venkatachalam, X. Jiang, T. Oldfield, and M. Waldman. *J Mol Graph Model 21*, 289-307 (2003).
34. A. Krammer, P. D. Kirchhoff, X. Jiang, C. M. Venkatachalam, and M. Waldman. *J Mol Graph Model 23*, 395-407 (2005).
35. D. K. Gehlhaar, G. M. Verkhivker, P. A. Rejto, C. J. Sherman, D. B. Fogel, L. J. Fogel, and S. T. Freer. *Chem Biol 2*, 317-324 (1995).
36. B. Ploeger, T. Mensinga, A. Sips, W. Seinen, J. Meulenbelt, and J. DeJongh. *Drug Metab Rev 33*, 125-147 (2001).
37. H. Hayashi, E. Miwa, and K. Inoue. *Biol Pharm Bull 28*, 161-164 (2005).

Date Received: November 24, 2010

Communicated by the Editor Ramaswamy H. Sarma